



## *In-silico* approaches to detect inhibitors of the human severe acute respiratory syndrome coronavirus envelope protein ion channel

Manoj Kumar Gupta<sup>a</sup> , Sarojamma Vemula<sup>b</sup>, Ravindra Donde<sup>c</sup>, Gayatri Gouda<sup>c</sup>, Lambodar Behera<sup>c</sup> and Ramakrishna Vadde<sup>a</sup> 

<sup>a</sup>Department of Biotechnology & Bioinformatics, Yogi Vemana University, Kadapa, Andhra Pradesh, India; <sup>b</sup>Department of Microbiology, Government Medical College, Anantapur, Andhra Pradesh, India; <sup>c</sup>ICAR-National Rice Research Institute, Cuttack, Odisha, India

Communicated by Ramaswamy H. Sarma

### ABSTRACT

Recent outbreak of Coronavirus disease (COVID-19) pandemic around the world is associated with 'severe acute respiratory syndrome' (SARS-CoV2) in humans. SARS-CoV2 is an enveloped virus and E proteins present in them are reported to form ion channels, which is mainly associated with pathogenesis. Thus, there is always a quest to inhibit these ion channels, which in turn may help in controlling diseases caused by SARS-CoV2 in humans. Considering this, in the present study, authors employed computational approaches for studying the structure as well as function of the human 'SARS-CoV2 E' protein as well as its interaction with various phytochemicals. Result obtained revealed that  $\alpha$ -helix and loops present in this protein experience random movement under optimal condition, which in turn modulate ion channel activity; thereby aiding the pathogenesis caused via SARS-CoV2 in human and other vertebrates. However, after binding with Belachinal, Macaflavanone E, and Vibsanol B, the random motion of the human 'SARS-CoV2 E' protein gets reduced, this, in turn, inhibits the function of the 'SARS-CoV2 E' protein. It is pertinent to note that two amino acids, namely VAL25 and PHE26, play a key role while interacting with these three phytochemicals. As these three phytochemicals, namely, Belachinal, Macaflavanone E & Vibsanol B, have passed the ADMET (Absorption, Distribution, Metabolism, Excretion and Toxicity) property as well as 'Lipinski's Rule of 5s', they may be utilized as drugs in controlling disease caused via SARS-COV2, after further investigation.

**Abbreviations:** NVT: constant number of particles, pressure and temperature; MD: molecular dynamics; NMR: nuclear magnetic resonance; FEL: free-energy landscape; LINCS: linear constraint solver; MDS: molecular dynamic simulations; RMSF: root mean square fluctuations;; RMSD: root mean square deviation;; NPT: constant number of particles, volume, and temperature; GMXAPBS: GROMACS tool to perform MM/PBSA; SDF: structure data file; MM/PBSA: molecular mechanics/Poisson-Boltzmann surface area

### ARTICLE HISTORY

Received 24 March 2020  
Accepted 30 March 2020

### KEYWORDS

Coronaviruses; severe acute respiratory syndrome; docking; modeling; molecular dynamics

### Introduction

Coronaviruses (CoVs) are responsible for causing numerous diseases in broad ranges of vertebrates, including humans. Though earlier, CoVs were only associated with a common cold, for the first time in 2002, new CoVs related to the 'severe acute respiratory syndrome' (SARS-CoV) discovered in the human population of China and caused the death of 10% of the total cases worldwide (Perlman & Netland, 2009; Rota et al., 2003). Recently, in December 2019, numerous patients from Wuhan, China, reported regarding symptoms like pneumonia. However, initially it was identified as novel coronavirus, namely, 2019-nCoV. Later, the World Health Organization (WHO) renamed that virus as 'severe acute respiratory syndrome coronavirus 2' (SARS-CoV2) and the disease caused by them is known as 'coronavirus disease 2019' (COVID-19). On March 11, 2020, the WHO officially

declared the outbreak of COVID-19 as a pandemic (Ramphul & Mejias, 2020). On March 28, 2020, 614169 confirmed cases with 28239 deaths and 933 confirmed cases are reported in India with 20 deaths (<https://mohfw.gov.in> & WHO). Thus, there is an urgent requirement to understand the virulence mechanisms associated with these pathogens, which in turn permits the development of more effective remedies for early prevention as well as controlling future outbreaks.

The SARS-CoV2 is an enveloped virus that belongs to the Coronaviridae family (Ramphul & Mejias, 2020). CoVs assemble together nearby intracellular membranes within the Endoplasmic reticulum-Golgi intermediate compartment (or ERGIC) after infection. Here they sprout within the lumen and consequently conveyed outside the cell through 'exocytosis' within the cargo vesicles (Krijnse-Locker et al., 1994; Tooze & Tooze, 1985). It is comprised of a positive-

strand RNA genome of size 29.7 kb and encodes a viral replicase that is associated with the novel genome synthesis and generation of a 'nested set of sub-genomic messenger RNAs, encoding both structural proteins present in all CoVs: Spike (S), Envelope (E), Membrane (M) and Nucleoprotein (N), and a group of proteins specific for SARS-CoV: 3a, 3b, 6, 7a, 7b, 8a, 8b, and 9b'(Nieto-Torres et al., 2014). While M and S protein constitutes the major portion of the viral envelope, E proteins are reported to oligomerize and form ion channels (Venkatagopalan et al., 2015). The E protein is located along with S-spike glycoprotein (Li et al., 2020), where it played a significant role in the assembly of the viral genome (Westerbeck & Machamer, 2019).

'SARS-CoV E' protein is a short, integral membrane protein comprised of 76–109 amino acids and its size range from 8.4 to 12 kDa. It starts with a short hydrophilic terminal followed by large hydrophobic transmembrane domain and terminates with long hydrophilic carboxyl end. Hydrophobic region oligomerise and form an ion-conductive pore in membranes. This protein plays a key role in various phases of the virus' life cycle, such as envelope formation, pathogenesis, budding and assembly (Ashour et al., 2020; Schoeman & Fielding, 2019). Few studies have also suggested that the 'SARS-CoV E' proteins' ion channel activity is modulated via pentameric ion channel (Pervushin et al., 2009). The 'SARS-CoV E' protein's ion channel activity is detected in the transmembrane region of the protein (Verdiá-Báguena et al., 2012; Wilson et al., 2004). Selectivity, as well as ion conductance associated with the E protein ion channel, are mostly modulated via the lipid membranes charge within which the pores aggregate. This, in turn, supports that 'lipid head-groups' are the main component of the structure of the channel facing the pore's lumen (Verdiá-Báguena et al., 2012, 2013).

Though the involvement of ion channels in CoVs pathogenesis remains a topic of debate, recently several studies have suggested that the absence of 'SARS-CoV E' protein results in an 'attenuated virus', thereby supporting that 'SARS-CoV E' protein is mainly responsible for pathogenesis (Pervushin et al., 2009; Regla-Nava et al., 2015). The involvement of other proteins of SARS-CoV in pathogenesis remains unclear to date (Venkatagopalan et al., 2015). Few studies have also reported that mutations within the extra-membrane domain of 'SARS-CoV E' protein disrupt the normal viral assembly as well as maturation (Fischer et al., 1998; Torres et al., 2007; Verdiá-Báguena et al., 2012). In transmissible gastroenteritis virus, the 'SARS-CoV E' protein deletion led to virus trafficking blockage within the secretory pathway as well as virus maturation (Curtis et al., 2002). Thus, the 'SARS-CoV E' protein serves as a key biomarker for preventing pathogenesis associated with the SARS-CoV (Pervushin et al., 2009).

For gaining detail insight into the structure & function, to date numerous 'three-dimensional' structures of the 'SARS-CoV E' protein have been deposited in the 'Protein Data Bank (PDB)'. Furthermore, as identifying novel drugs through laboratory approaches demands huge capital as well as investments, there is a continuous demand for screening

drug molecules via high screening computational methods that saves both money as well as time (Gupta, Donde, et al., 2019; Gupta & Vadde, 2020b; Gupta & Vadde, 2020a). Nevertheless, ADMET ('Absorption, Distribution, Metabolism, Excretion and Toxicity') as well as 'Lipinski's Rule of 5s' property passed natural drugs may have either minimum or no adverse-effects (Gupta et al., 2020; Gupta & Vadde, 2020a,b). Recently, genome of the first SARS-CoV2 (Wuhan-Hu-1) has also been successfully sequenced and submitted in GenBank (Accession no. MN908947.3) (Shang et al., 2020). By considering the above information, in the present study, authors employed computational approach for identifying the best possible structure of the 'SARS-CoV2 E' protein present in the PDB database to understand its structure and function as well as its behaviour towards various phytochemicals. This, in turn, may help us in identifying few phytochemicals that may inhibit the function of the 'SARS-CoV2 E' protein; thereby preventing the pathogenesis associated with SARS-CoV2. In the near future, these phytochemicals may serve as good contestants for treating diseases caused by SARS-CoV2 after further laboratory investigation.

## Methodology

### Sequence and structure download

The Uniprot was utilized for downloading the human 'SARS-CoV E' protein sequence (ID: P59637). The NCBI protein database was utilized for downloading the human 'SARS-CoV2 E' protein sequence (ID: YP\_009724392.1). Multalin, a web-based tool was implemented to detect difference between 'SARS-CoV E' and 'SARS-CoV2 E' protein. Subsequently, sequence of 'SARS-CoV2 E' protein was subjected to NCBI's utility 'BLASTp' (Altschul et al., 1990). Based on maximum sequence identity (81%), structure with PDB (Protein Data Bank) ID 5 × 29 is detected as the best homologous structure of human 'SARS-CoV2 E' protein. As the 'SARS-CoV E' protein function as a homopentamer (Pervushin et al., 2009), the complete structure of 5 × 29, comprised of five chains, was employed for downstream analysis.

### Molecular dynamic simulations (MDS): Phase I

To gain detail insight into the structural characteristic of the downloaded protein and removing any conflicts present between its atoms of main and side chain (Donde et al., 2019; Gouda et al., 2020; Gupta & Vadde, 2020b), MDS were employed using 'Gromos96-43a1 force field' of 'GROMACS 5.1' for 200 ns (Abraham et al., 2015). As 'SARS-CoV2 E' protein resides in a transmembrane region, at first, downloaded structure of 5 × 29 was embedded in the 'equilibrated bilayer of DPPC (dipalmitoylphosphatidylcholine)' using 'g\_membed' tool of 'GROMACS 5.1' (Wolf et al., 2010) using the aid of 'Berger lipids' derived parameters from 'Berger, Edholm, and Jahnig' (Berger et al., 1997). Further solvation of the entire system till energy minimization followed by equilibrating the complete system under NVT ('Constant Number of Particles, Pressure and Temperature') and NPT ('Constant Number of

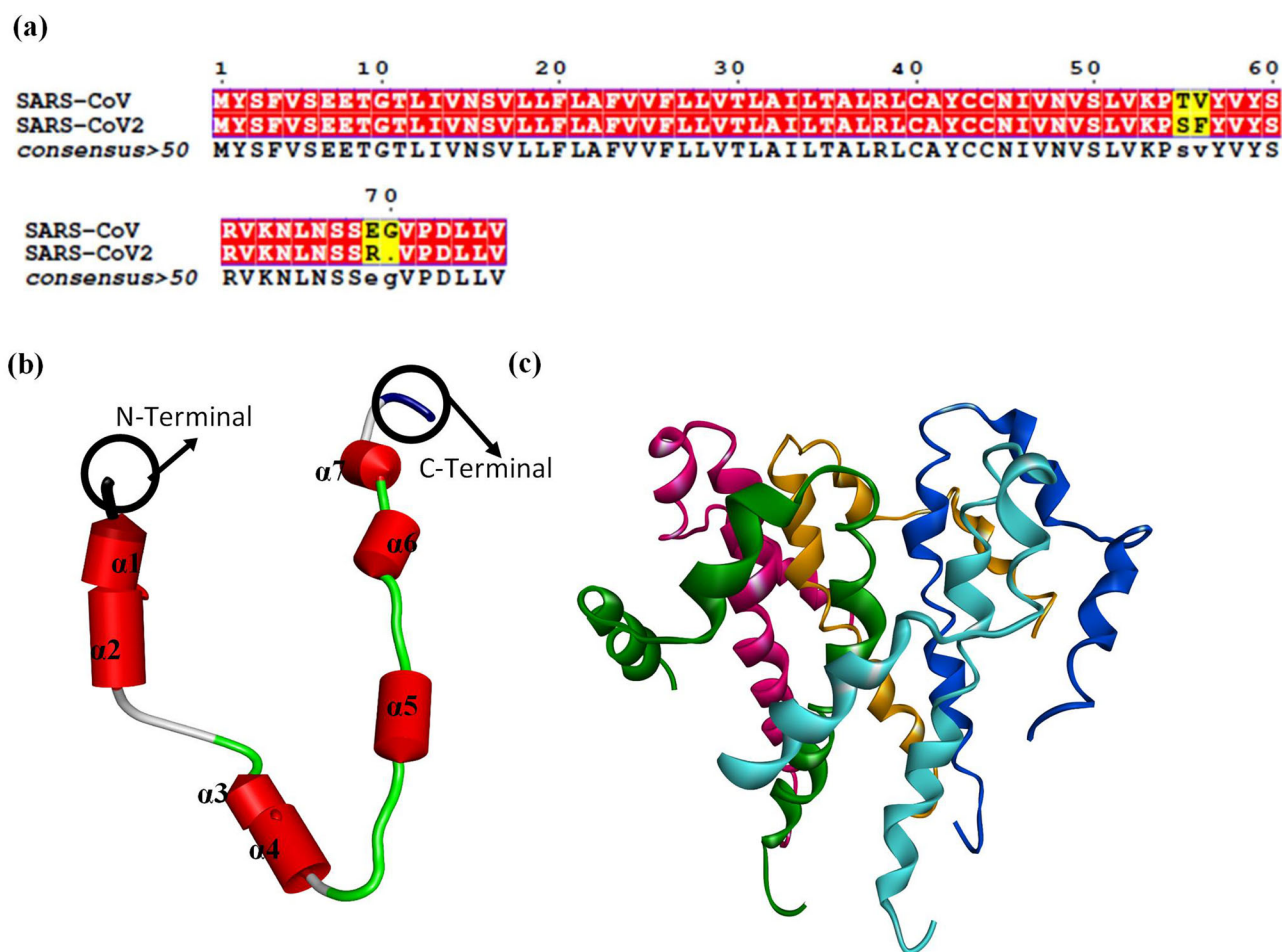


**Figure 1.** (a) Sequence similarity between protein sequence of ‘SARS-CoV E’ and ‘SARS-CoV2 E’ protein. 3D structure of ‘SARS-CoV2 E’ protein, (b) One unit is composed of only seven  $\alpha$ -helices and 8 loops. (c) Homopentamer. In (c), green, pink, orange, blue and cyan depicts chain A, B, C, D and E of the ‘SARS-CoV2 E’ pentameric protein.

Particles, Volume, and Temperature’) conditions were carried out as stated in detail at [http://www.md-tutorials.com/gmx/membrane\\_protein/index.html](http://www.md-tutorials.com/gmx/membrane_protein/index.html). Final molecular dynamic (MD) trajectories as well as the quality of simulations were analyzed via ‘GROMACS 5.1’ (Gupta & Vadde, 2020b). ‘Principal Component Analysis’ (PCA) was also carried out for capturing the most flexible area and the motion of the  $\alpha$ -helix & the  $\beta$ -strands present within the protein during 200 ns. Equilibrated conformers from the MD were used to produce the mean structure of the ‘SARS-CoV2 E’ protein (Gupta & Vadde, 2020b). Backbone atoms’ free energy for the ‘SARS-CoV2 E’ protein was calculated using the ‘GROMACS 5.1’ from 20 ns to 200 ns with 20 ns interval (Gupta & Vadde, 2020b).

### Preparation of ligands

‘Three-dimensional’ structure of 4153 phytochemicals having ‘drug-like’ features from our earlier published literatures (Gupta & Vadde, 2019a, 2020a,b) were employed in the present study. The DrugMint server The DrugMint server (Dhanda et al., 2013) was employed for detecting ADMET or ‘drug-like’ properties of each phytochemicals. DrugMint server predicts ADMET or drug-likelihood of any drug/phytochemicals using various classification models. All models were trained, tested and evaluated on a dataset comprised of 3206 experimental drugs and 1347

approved drugs of DrugBank 2.5. All QSAR models were developed using open source software packages like PaDEL, WEKA, SVM\_Light (Dhanda et al., 2013) ‘Three-dimensional’ structures of each phytochemicals were obtained from TIPdb database and have either anti-tuberculosis, anti-cancer, anti-platelet, or no therapeutic properties (Lin et al., 2013).

### Molecular docking

The active site pocket present in the ‘SARS-CoV2 E’ protein was calculated using the CASTp server (Binkowski et al., 2003). Active pocket with the highest volume as well as area was considered for molecular docking studies with phytochemicals having 250 conformations (Gupta, Vadde, et al., 2019; Gupta & Vadde, 2020b) via the AutoDock (Morris et al., 2009) tool. Three best phytochemical having the minimal binding energy was considered for further study (Gupta & Vadde, 2020b). Complex formation was done employing the ‘Discovery Studio’ Software (Biovia, 2017).

### MDS: Phase II

Amongst 250 conformations, the docking result of the ‘SARS-CoV2 E’ protein with three different phytochemicals having the minimal binding energy was considered for the 200 ns MDS,

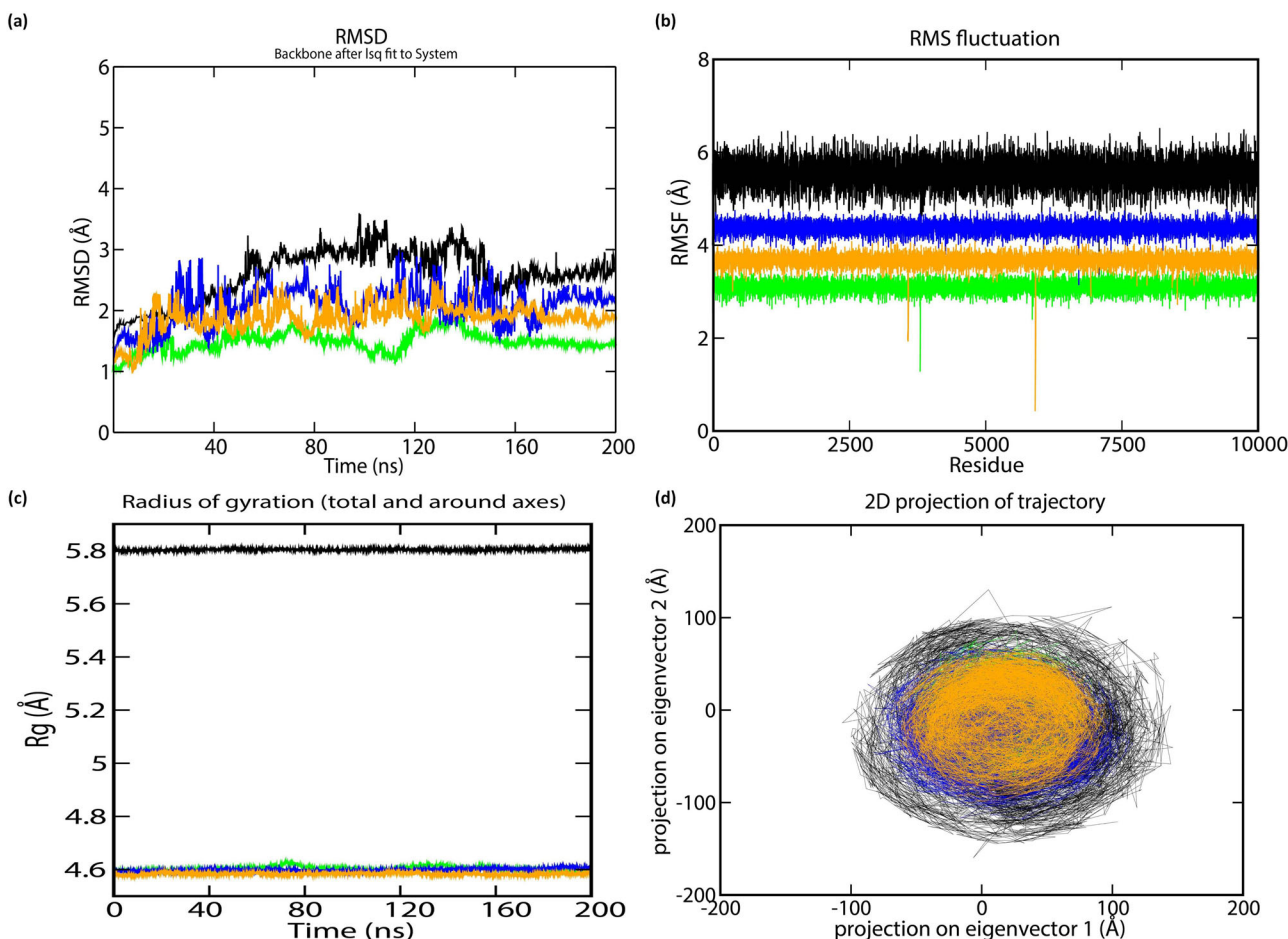


**Figure 2.** The stability parameters for ‘SARS-CoV E’ protein during 200 ns: (a) RMSD of C- $\alpha$  (b) RMSF of C- $\alpha$  (c) Radius of gyration of C- $\alpha$ , and (d) Principle Component Analysis (PCA) of  $\alpha$ -helix and  $\beta$ -strand movement. The trajectory projected to the two-dimensional space. Black, light green, blue, and orange lines represent ‘SARS-CoV2 E’ protein and Complexes A, B & C during 200 ns, respectively.

separately (Gupta & Vadde, 2020). The PRODRG server (Schüttelkopf & van Aalten, 2004) was employed for generating the ligand’s topology parameters. Subsequently, complete MDS was performed as described above in the *MDS: Phase I*.

### MM/PBSA calculations

Using the GMXAPBS utility of the ‘GROMAC 5.1’, 2000 snapshots were retrieved from the MD trajectories of all the three complexes, individually, to calculate the binding free energy from 20 to 200 ns with 20 ns interval (Gupta & Vadde, 2020b).

### Inter-molecular interaction studies

Inter-molecular interactions present within the three complexes after 200 ns MDS were performed via Discovery Studio (Gupta & Vadde, 2020b).

## Results and discussion

### Protein model

Comparative sequence analysis via Multalin reveals that ‘SARS-CoV E’ and ‘SARS-CoV2 E’ protein sequence share

94.74% identity amongst themselves. The ‘three-dimensional’ structure of one unit of ‘SARS-CoV2 E’ comprised of only seven  $\alpha$ -helices and eight loops (Figure 1(a)). As there are five homo-units, the complete structure of ‘SARS-CoV2 E’ consists of 35  $\alpha$ -helices and 40 loops (Figure 1(b)). As the ‘SARS-CoV E’ proteins’ ion channel activity is modulated via pentameric ion channel (Pervushin et al., 2009), complete structure comprising of five subunits was employed for the downstream analysis.

### MDS: Phase I

To understand the structural characteristics of the ‘SARS-CoV2 E’ protein, MD trajectories of 200 ns were analyzed (Gupta & Vadde, 2020b). The obtained result revealed that during 200 ns, potential energy fluctuates within  $-2785852.25$  &  $-1717123.84$  kJ/mol. Pressure fluctuates within  $-311.56$  bar &  $338.38$  bar with an average value  $1.75$  bar. The temperature fluctuates within  $296.97$  K &  $303.30$  K with an average value of  $299.99$  K. Density fluctuates within  $973.57$  &  $991.84$  kg/m<sup>3</sup> with an average value  $980.78$  kg/m<sup>3</sup>. Root mean square deviation (RMSD) & root mean square fluctuation (RMSF) of C $\alpha$  atoms as a function of residue number and radius of gyration (Rg) as a function of simulation time (Donde et al., 2019; Gouda et al., 2020;

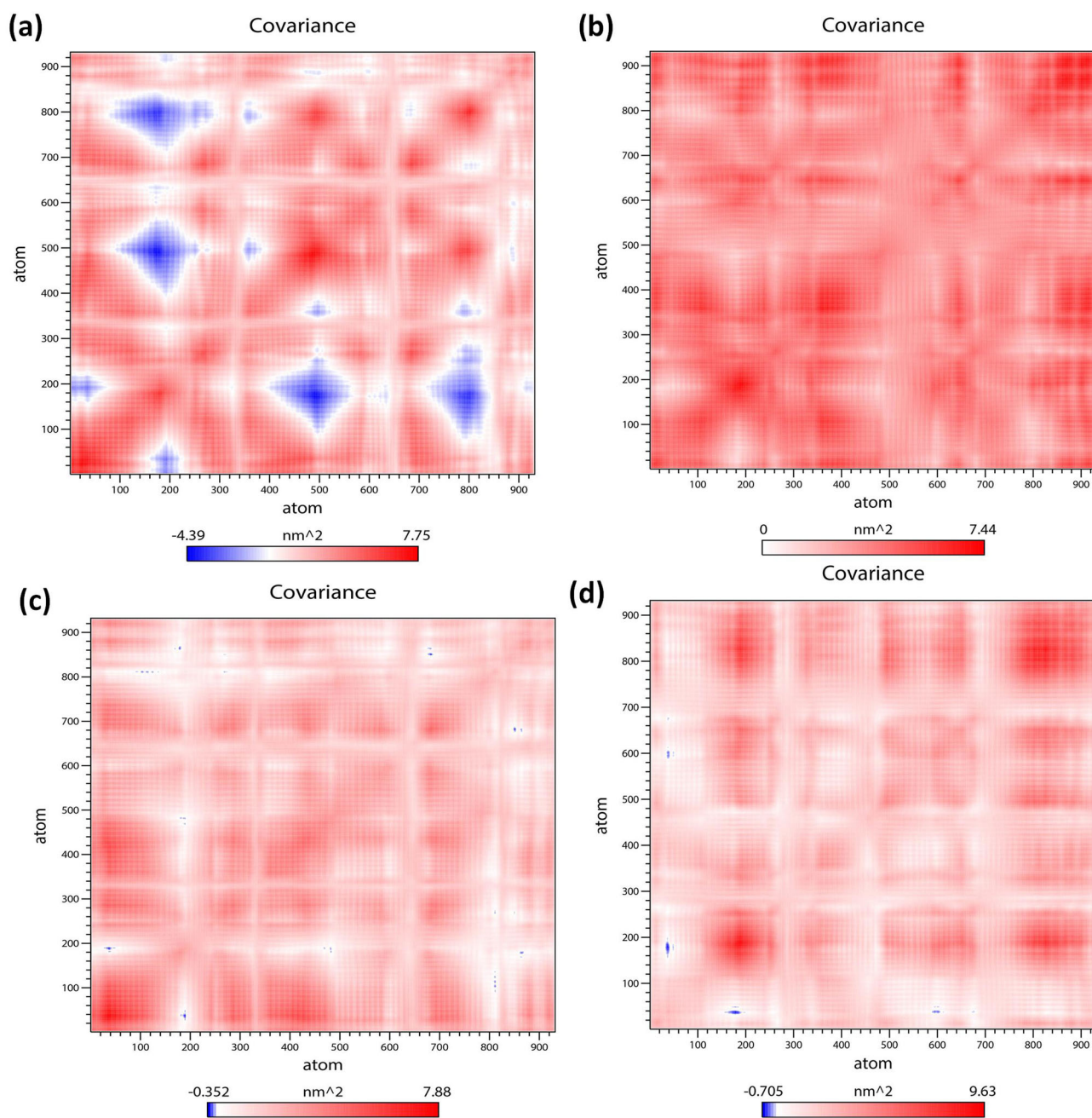


**Figure 3.** Comparative study of cross-correlation matrices of C- $\alpha$  atoms of modeled (a) 'SARS-CoV2 E' protein (b) Complex A (c) Complex B and (d) Complex C during 200 ns simulation. The range of motion indicated by various colors in the panel. Red indicates a positive correlation, whereas blue indicates anti-correlation.

Gupta et al., 2018; Mehrnejad & Chaparzadeh, 2008; Rani & Lakshmi, 2019; Tandon et al., 2015) were employed for estimating the protein stability during the MD analysis. The average RMSD value of the protein backbone atoms is estimated to be 2.74 Å (Figure 2(a)). RMSD is found to be stable subsequently 170 ns. The value of RMSF fluctuates within 4 Å & 6.3 Å with an average value of 5.96 Å. Amino acids that undergo maximum fluctuation during 200 ns MDS were VAL17, ALA22, LEU19, LEU27, PHE23, PHE26, LEU27, VAL24, VAL25, VAL29, ILE33, ALA36 and TYR42 (i.e. RMSF > 6 nm). As these residues play an important role during protein-ligand interaction, they may serve as a biomarker during the drug discovery process (Gouda et al., 2020; Gupta & Vadde, 2019a, 2020a, 2020b) (Figure 2(b)). The Rg values of the

protein (Figure 2(c)), fluctuates within 5.81 Å & 5.83 Å with an average value of 5.82 Å; thereby supporting its condensed architecture as well as size (Donde et al., 2019; Gupta & Vadde, 2019b). Result obtained from the PCA analysis suggests the random movement of the 'SARS-CoV2 E' protein (Figure 2(d)) throughout the 200 ns MDS. Mean number of 'intra-protein' hydrogen bond & 'inter-hydrogen' bond formed between 'SARS-CoV2 E' protein & water is 1.98 and 1.98, respectively. 'Cross-correlation matrix' of the C- $\alpha$  displacement revealed that all residues present within the 'SARS-CoV2 E' protein experience both negative (depicted via blue shades) as well as positive correlated motions (depicted via red shades) (Figure 3(a)), which in turn support random movement of the 'SARS-CoV2 E' protein. This finding is also

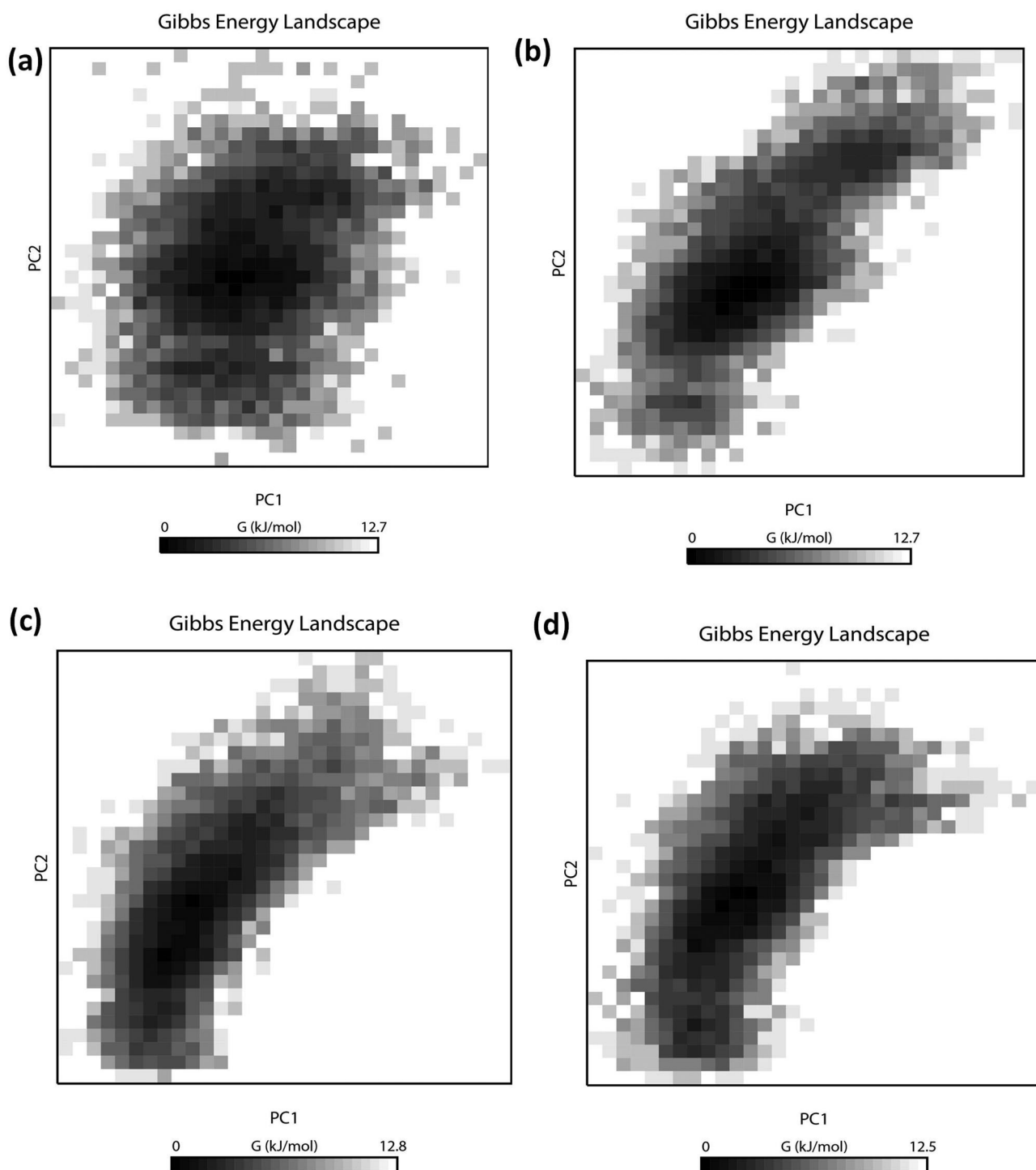


**Figure 4.** Projections of the free energy landscape of (a) 'SARS-CoV2 E' protein (b) Complex A (c) Complex B and (d) Complex C during 200 ns simulation. Various colors in the panel indicate the range of motion, where dark black indicates the lowest energy configuration, and white shows the highest energy configuration.

in accordance with the 'free energy landscape' analysis (Figure 4(a)). Minimal energy associated with the FEL for the 'SARS-CoV2 E' protein at 20 to 200 ns with difference of 20 ns are 0.20, 0.28, 0.32, 0.38, 0.41, 0.41, 0.43, 0.43, 0.45 and 0.49 kcal/mol respectively.

The random movement of the 'SARS-CoV2 E' protein indicates its involvement in the ion channels. This is in accordance with earlier studies where authors have reported that the ion channel activity of 'SARS-CoV2 E' proteins is modulated via pentameric ion channel (Pervushin et al., 2009). It is

pertinent to note that the structure of 'SARS-CoV2 E' protein becomes stable after 170 ns. Hence, the average structure of the 'SARS-CoV2 E' protein was obtained from the stable plateau of the RMSD after 170 ns for downstream analysis.

#### **Molecular docking with phytochemicals**

Further, the CASTp server was employed for detecting the active site present within the 'SARS-CoV2 E' protein. The

**Table 1.** Free binding energy (Kcal/mol) scores of the best ten interacting phytochemicals with 'SARS-CoV2 E' protein.

ID	Phytochemical	Plant source	Inhibition constant	vdW + H bond + desolv Energy (kcal/mol)	Final total internal energy (kcal/mol)	Torsional free energy (kcal/mol)	Final intermolecular energy (kcal/mol)	Electrostatic energy (kcal/mol)	Free energy of binding (kcal/mol)	Unbound system's energy (kcal/mol)
TIP006452	Belachinal	<i>Belamcanda chinensis</i>	3.99 nM (nanomolar)	-12.37	-2.49	0.89	-12.35	0.02	-11.46	-2.49
TIP005365	Macafllavanone E	<i>Macaranga tanarius</i>	7.71 nM (nanomolar)	-12.01	-1.42	0.89	-11.96	0.05	-11.07	-1.42
TIP003272	Vibsanol B	<i>Viburnum odoratissimum</i>	7.62 nM (nanomolar)	-11.92	-1.53	0.89	-11.97	-0.05	-11.07	-1.53
TIP003258	14R*, 15-Epoxyvibsanin C	<i>Viburnum odoratissimum</i>	18.24 nM (nanomolar)	-11.46	-2.04	0.89	-11.45	0.01	-10.56	-2.04
TIP005363	Macafllavanone C	<i>Macaranga tanarius</i>	20.45 nM (nanomolar)	-11.34	-1.56	0.89	-11.38	-0.04	-10.49	-1.56
TIP000749	Luzonoid D	<i>Viburnum luzonicum</i>	21.26 nM (nanomolar)	-11.39	-2.14	0.89	-11.36	0.02	-10.47	-2.14
TIP008605	Grossamide K	<i>Hibiscus cannabinus</i>	20.01 nM (nanomolar)	-11.33	-2.05	0.89	-11.4	-0.07	-10.50	-2.05
TIP009461	(-)-Blestriarene C	<i>Crematstra appendiculata</i>	23.82 nM (nanomolar)	-11.27	-1.77	0.89	-11.29	-0.02	-10.40	-1.77
TIP005366	Macafllavanone F	<i>Macaranga tanarius</i>	25.33 nM (nanomolar)	-11.24	-1.45	0.89	-11.26	-0.02	-10.36	-1.45
TIP005783	Dolichosterone	<i>Oryza sativa</i> and <i>Zea mays</i>	27.52 nM (nanomolar)	-11.19	-1.46	0.89	-11.21	-0.02	-10.31	-1.46

obtained result revealed that the highest volume and area of the binding cavity within the 'SARS-CoV2 E' protein is 7625.969 Å<sup>3</sup> & 7163.067 Å<sup>2</sup>, respectively. Forty-four amino acids that are involved in the formation of the active site are GLU8, THR11, LEU12, VAL14, ASN15, VAL17, LEU18, LEU19, PHE20, LEU21, ALA22, PHE23, VAL24, VAL25, PHE26, LEU27, LEU28, VAL29, THR30, LEU31, ALA32, ILE33, LEU34, THR35, ALA36, LEU37, ARG38, LEU39, ALA40, TYR42, ALA43, ALA44, ILE46, VAL47, VAL49, LEU51, PRO54, VAL56, TYR57, SER60, ARG61, LYS63, ASN64 and LEU65. Subsequently, molecular docking between the protein and ligand with 250 conformations was performed using the AutoDock tool. 126 × 126 × 126 was assigned as a grid box with a grid center of -0.496, 0.0 and 0.0. The grids were selected very carefully for allocating active sites along with the surrounding surface's major area (Donde et al., 2019; Gouda et al., 2020; Gupta, Vadde, et al., 2019).

Subsequently, molecular docking of the 'SARS-CoV2 E' protein with ligands having 250 conformations using the AutoDock tool revealed that the best ten phytochemicals with minimal binding energy are TIP006452 (Belachinal), TIP005365 (Macafllavanone E), TIP003272 (Vibsanol B), TIP003258 (14 R\*, 15-Epoxyvibsanin C), TIP005363 (Macafllavanone C), TIP000749 (Luzonoid D), TIP008605 (Grossamide K), TIP009461 ((-)-Blestriarene C), TIP005366 (Macafllavanone F) and TIP005783 (Dolichosterone). Binding energy of 'SARS-CoV2 E' protein with TIP006452, TIP005365, TIP003272, TIP003258, TIP005363, TIP000749, TIP008605, TIP009461, TIP005367, TIP005366 and TIP005783 is -11.46 kcal/mol, -11.07 kcal/mol, -11.07 kcal/mol, -10.56 kcal/mol, -10.49 kcal/mol, -10.47 kcal/mol, -10.50 kcal/mol, -10.40 kcal/mol, -10.40 kcal/mol, -10.36 kcal/mol and -10.31 kcal/mol, respectively (Supplementary File I and Table 1). Binding energy of all 4153 phytochemicals is depicted in the Supplementary File I. Earlier one study has reported that Macafllavanone C may be utilized for treating Alzheimer's disease (Gupta & Vadde, 2019a). In 2016, Teponno and the team reported about the anti-melanogenic property of the Grossamide K (Bertrand Teponno et al., 2016). Earlier Seo and his team have also reported that compounds present in the ethyl acetate fraction of *Sanguisorba officinalis*, namely euphormisin M3, arjunglucoside II, pomolic acid-3-β-O-α-L-arabionopyranoside, 3,3'-di-O-methylellagic acid, 3,8-dihydroxy-4,10-dimethoxy-7-oxo-[2] benzopyrono [4,3-b][1]benzopyran-7-(5H)-one, chikusetsusaponin II, deglucose chikusetsusaponin Iva, belachinal, irilone and ellagic acid, may have the inhibitory effect on inflammasome pathways and protective role in endotoxin-induced septic shock. However, to best of our knowledge, no medicinal properties have been assigned to rest seven phytochemicals, namely, Macafllavanone E, Vibsanol B, '14 R\*, 15-Epoxyvibsanin C', Luzonoid D, (-)-Blestriarene C, Macafllavanone F and Dolichosterone. As three compounds, namely, Belachinal, Macafllavanone E and Vibsanol B, have the minimal binding energy with the 'SARS-CoV2 E' protein (Table 1), three separate complexes between 'SARS-CoV2 E' protein and each ligand were done separately using Discovery Studio Software. The complex of the 'SARS-CoV2 E' protein with Belachinal, Macafllavanone E and Vibsanol B, separately, will be known as Complex A, B and C, respectively, henceforth.

**Table 2.** Final binding energy (kJ/mol) between protein and phytochemicals, obtained through MM/PBSA estimation, in Complex AC from 20 to 200 ns with 20 ns interval.

Complex	Time (ns)	van der Waal energy (kJ/mol)	SASA energy (kJ/mol)	Binding energy (kJ/mol)	Electrostatic energy (kJ/mol)	Polar solvation energy (kJ/mol)
Complex A	20	-232.399 ± 2.692	-20.992 ± 0.209	-208.518 ± 2.314	-49.745 ± 0.550	94.580 ± 1.079
	40	-250.391 ± 1.490	-22.075 ± 0.114	-225.224 ± 1.310	-51.492 ± 0.314	98.747 ± 0.575
	60	-258.354 ± 1.064	-22.744 ± 0.081	-232.717 ± 0.940	-53.110 ± 0.231	101.502 ± 0.402
	80	-262.304 ± 0.831	-23.106 ± 0.064	-236.226 ± 0.733	-54.292 ± 0.190	103.475 ± 0.324
	100	-266.681 ± 0.679	-23.450 ± 0.053	-239.571 ± 0.612	-54.877 ± 0.167	105.424 ± 0.284
	120	-269.779 ± 0.617	-23.693 ± 0.047	-242.226 ± 0.542	-55.629 ± 0.152	106.884 ± 0.244
	140	-270.669 ± 0.513	-23.759 ± 0.041	-243.042 ± 0.466	-56.199 ± 0.132	107.598 ± 0.218
	160	-276.545 ± 0.377	-24.012 ± 0.027	-245.952 ± 0.311	-56.694 ± 0.089	111.303 ± 0.178
	180	-281.613 ± 0.517	-24.198 ± 0.035	-248.422 ± 0.405	-57.253 ± 0.119	114.619 ± 0.268
	200	-286.018 ± 0.355	-24.385 ± 0.023	-250.979 ± 0.272	-57.657 ± 0.080	117.087 ± 0.186
Complex B	20	-194.989 ± 1.504	-18.758 ± 0.149	-169.711 ± 1.457	-14.672 ± 0.392	58.713 ± 0.751
	40	-204.767 ± 0.906	-19.490 ± 0.083	-181.077 ± 0.887	-15.313 ± 0.237	58.485 ± 0.464
	60	-212.452 ± 0.729	-20.226 ± 0.067	-186.884 ± 0.680	-16.890 ± 0.190	62.672 ± 0.437
	80	-222.140 ± 0.694	-20.890 ± 0.058	-194.731 ± 0.633	-17.348 ± 0.151	65.650 ± 0.378
	100	-231.827 ± 0.709	-21.409 ± 0.052	-201.292 ± 0.595	-18.737 ± 0.143	70.692 ± 0.383
	120	-240.733 ± 0.704	-21.884 ± 0.049	-207.375 ± 0.553	-19.845 ± 0.133	75.075 ± 0.375
	140	-245.532 ± 0.650	-22.073 ± 0.044	-211.410 ± 0.517	-20.433 ± 0.123	76.615 ± 0.337
	160	-246.434 ± 0.406	-22.105 ± 0.027	-212.651 ± 0.332	-20.695 ± 0.079	76.567 ± 0.214
	180	-246.422 ± 0.524	-22.060 ± 0.036	-212.942 ± 0.429	-20.864 ± 0.103	76.387 ± 0.276
	200	-248.494 ± 0.343	-22.219 ± 0.024	-214.938 ± 0.280	-21.055 ± 0.065	76.820 ± 0.178
Complex C	20	-254.979 ± 2.304	-22.542 ± 0.125	-239.349 ± 2.110	3.371 ± 0.231	34.849 ± 0.706
	40	-286.216 ± 1.576	-24.151 ± 0.086	-248.460 ± 1.145	-3.150 ± 0.301	65.013 ± 1.248
	60	-303.324 ± 1.269	-25.038 ± 0.067	-251.388 ± 0.815	-7.891 ± 0.275	84.866 ± 1.122
	80	-313.068 ± 1.029	-25.344 ± 0.053	-253.574 ± 0.625	-10.362 ± 0.231	95.204 ± 0.929
	100	-322.209 ± 0.905	-25.579 ± 0.045	-256.632 ± 0.533	-11.477 ± 0.193	102.636 ± 0.812
	120	-317.991 ± 1.281	-24.957 ± 0.088	-249.991 ± 0.943	-11.753 ± 0.171	104.741 ± 0.771
	140	-301.108 ± 1.711	-23.549 ± 0.128	-234.943 ± 1.447	-11.302 ± 0.150	101.072 ± 0.740
	160	-267.273 ± 1.495	-20.882 ± 0.116	-207.250 ± 1.261	-10.046 ± 0.104	90.990 ± 0.576
	180	-261.003 ± 2.103	-20.275 ± 0.163	-202.484 ± 1.800	-9.884 ± 0.136	88.642 ± 0.777
	200	-254.047 ± 1.497	-19.626 ± 0.114	-197.457 ± 1.236	-9.794 ± 0.091	86.053 ± 0.539

### MDS: Phase II

For gaining detail insight into the structural characteristics of Complex A to C separately, MD trajectories of each three complexes for 200 ns were analyzed separately through 'GROMACS5.1'. The obtained result revealed that during 200 ns, in Complex A potential energy fluctuates within -4305011.50 & -3247362.33 kJ/mol. Pressure fluctuates within -397.76 bar & 379.10 bar with an average value 2.74 bar. Density fluctuates within 986.89 & 1000.63 kg/m<sup>3</sup> with an average value 993.64 kg/m<sup>3</sup>. In Complex B, potential energy fluctuates within -3524890.12 & -2435552.00 kJ/mol. Pressure fluctuates within -369.94 bar & 349.67 bar with an average value 2.32 bar. Density fluctuates within 982.12 & 999.99 kg/m<sup>3</sup> with an average value 986.74 kg/m<sup>3</sup>. In Complex C, potential energy fluctuates within -3311430.25 & -2095840.00 kJ/mol. Pressure fluctuates within -349.38 bar & 376.10 bar with an average value 2.15 bar. Density fluctuates within 979.40 & 995.38 kg/m<sup>3</sup> with an average value 982.81 kg/m<sup>3</sup>. In all three complexes, the temperature fluctuates within ~295.24 K & ~304.98 K with an average value of 300.00 K. Average RMSD value of the protein backbone atoms in Complex A-C is estimated to be 1.75 Å, 2.16 Å and 2.56 Å, respectively (Figure 2(a)). RMSD in all the three complexes is found to be stable subsequently 180 ns. The Rg values of all three complexes (Figure 2(c)) support their condensed architecture as well as size (Gupta & Vadde, 2020). Minimal energy associated with the FEL for the Complex A at 20 to 200 ns with difference of 20 ns are 0.26, 0.36, 0.25, 0.31, 0.35, 0.37, 0.40, 0.42, 0.42, 0.43, 0.44 & 0.44 kcal/mol respectively. Minimal energy associated with the FEL for the Complex B at 20 to 200 ns with difference of 20 ns

are 0.26, 0.31, 0.31, 0.37, 0.38, 0.40, 0.41, 0.43, 0.45 & 0.45 kcal/mol respectively. Minimal energy associated with the FEL for the Complex C at 20 to 200 ns with difference of 20 ns are 0.26, 0.36, 0.37, 0.39, 0.40, 0.41, 0.42, 0.42, 0.44 & 0.47 kcal/mol, respectively. Result obtained from the PCA analysis suggests that the movement of Complex A < Complex B < Complex C < 'SARS-CoV2 E' protein (Figure 2(d)). This might be due to decreased potential energy and increased pressure in all the three complexes, which in turn supports that the random movement of the 'SARS-CoV2 E' protein decrease after binding with these phytochemicals (Figure 2(d)); thereby supporting that these three phytochemicals may function as drugs for treating or controlling diseases caused via SARS-CoV2 in human.

### MM/PBSA calculations for ligand binding affinities

The obtained result revealed that the final binding energy of Complex A (-250.979 ± 0.272 kJ/mol) < Complex B (-214.938 ± 0.280 kJ/mol) < Complex C (-197.457 ± 1.236 kJ/mol). The overall distribution of electrostatic, SASA (Solvent Accessible Surface Areas), van der Waal, polar solvation, and final, binding energy from 20 ns to 200 ns with 20 ns interval of Complex A to C complexes are depicted in Table 2.

### Intermolecular interaction studies

Intermolecular interaction study in all the three complexes, separately, via Discovery Studio, suggests that amino acid involved in the intermolecular interaction of Complex A with

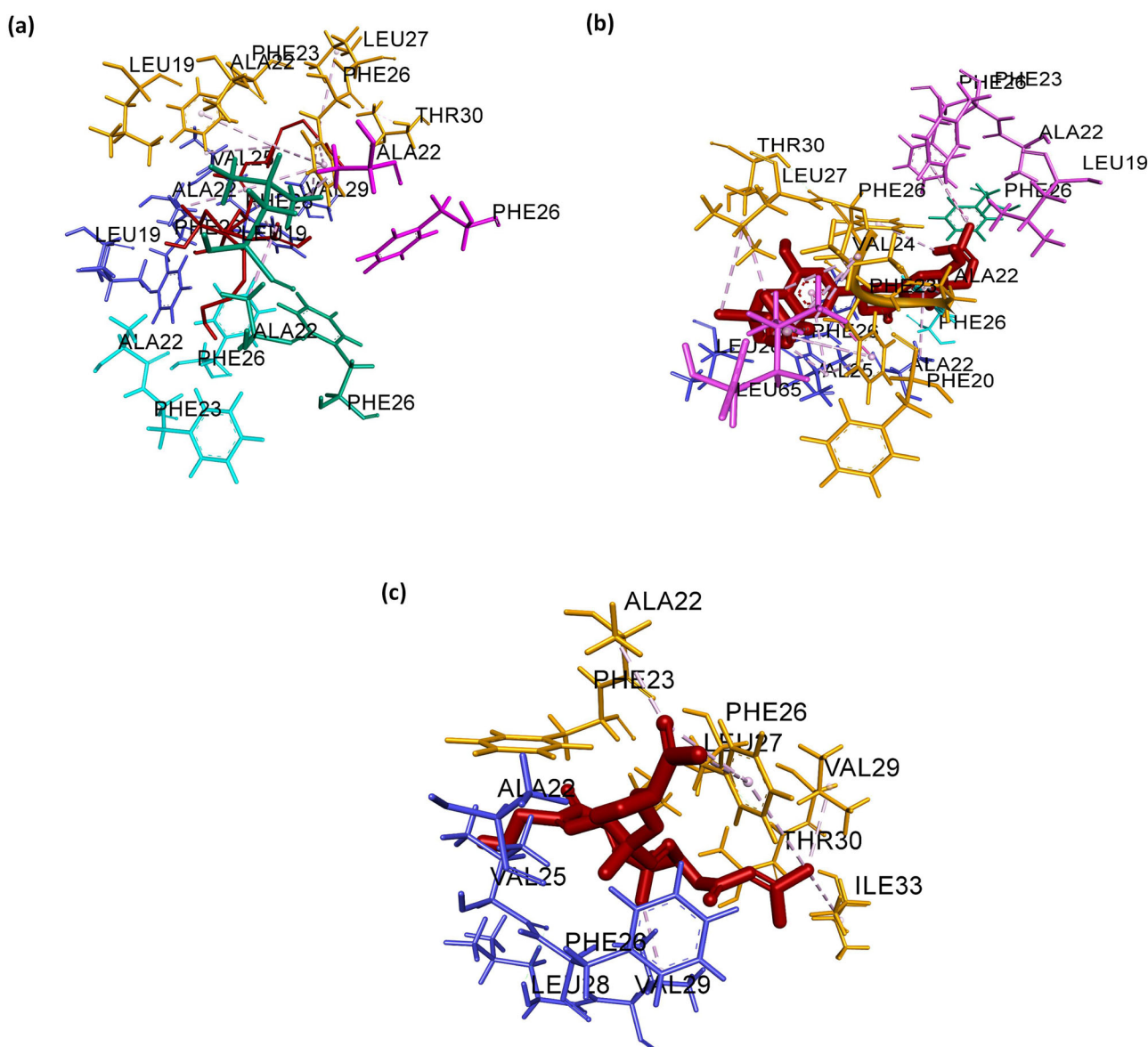


**Figure 5.** ‘Three-dimensional’ representation of intermolecular interaction in (a) Complex A, (b) Complex B and (c) Complex C. Green, pink, orange, blue and cyan depicts chain A, B, C, D and E of the pentameric ‘SARS-CoV2 E’ protein, respectively. Dark brown depicts ligand.

ligands, are LEU19, ALA22, PHE23, VAL25, PHE26 and VAL29. Ten hydrophobic bonds C:ALA22 -: TIP006452:C, D:ALA22 -: TIP006452:C; TIP006452:C - C:LEU19; TIP006452:C - D:VAL25; TIP006452:C - D:VAL29; TIP006452:C - D:VAL29; TIP006452:C - D:VAL29, C:PHE23 -: TIP006452:C, C:PHE26 -: TIP006452:C and D:PHE26 -: TIP006452:C) are formed. Hydrophobic bond length ranges from 4.30 Å to 5.90 Å (Figure 5(a)). Amino acid involved in the intermolecular interaction of Complex B with ligands, are PHE23, VAL24, VAL25, PHE26, LEU27 and LEU65. Fourteen hydrophobic bonds (C:PHE23 -: TIP005365; D:VAL25 -: TIP005365; TIP005365:C - C:LEU27; TIP005365:C - C:VAL24; TIP005365:C - C:LEU27; TIP005365:C - B:LEU65; TIP005365:C - C:VAL24, A:PHE26 -: TIP005365:C, B:PHE26 -: TIP005365:C, C:PHE23 -: TIP005365, C:PHE26 -: TIP005365:C; TIP005365 - C:ALA22; TIP005365 - D:ALA22 and TIP005365 - D:VAL25) are formed. Hydrophobic bond length ranges from 3.81 Å to 5.31 Å (Figure 5(b)). Amino acid involved in the intermolecular interaction of Complex C with ligands, are ALA22, VAL25,

PHE26, VAL29 and ILE33. Nine hydrophobic bonds (C:THR30:HG1 -: TIP003272:O; TIP003272:H - D:ALA22:O, D:VAL25 -: TIP003272, D:VAL29 -: TIP003272; TIP003272:C - D:VAL25; TIP003272:C - D:VAL29; TIP003272:C - C:ILE33, C:PHE23 - D:VAL25, D:PHE26 -: TIP003272:C,) are formed. Hydrophobic bond length ranges from 3.02 Å to 5.90 Å (Figure 5(c)). No hydrogen and electrostatic bonds is found in either of the three complexes.

In all the three complexes, amino acids present in the chain C and D mostly bind with ligands. Amino acids, namely VAL25 and PHE26 helps in bond formation in all three complexes. It is pertinent to note that these amino acids also experience the maximum RMSF during 200 ns simulation in the ‘SARS-CoV2 E’ protein; thereby suggesting their importance during protein-ligand interaction. Thus, in the near future, these amino acids present in the chain C and D of the ‘SARS-CoV2 E’ protein may serve as a biomarker for controlling pathogenesis caused via SARS-CoV2 in human.

## Conclusion

In conclusion, the publically available structure of the human 'SARS-CoV2 E' protein was downloaded and employed to study its structure and function as well as its interaction with various phytochemicals using computational approaches. Results obtained revealed that the human 'SARS-CoV2 E' is a pentameric protein comprised of 35  $\alpha$ -helices and 40 loops. During 200 ns,  $\alpha$ -helix and loops present in this protein experiences random movement, which in turn modulate normal ion channel activity; thereby aiding the pathogenesis caused via SARS-CoV2 in human and other vertebrates. However, after binding with Belachinal, Macaflavanone E, and Vibsanol B, the random motion of the human 'SARS-CoV2 E' protein gets reduced; this, in turn, inhibits the function of the human 'SARS-CoV2 E' protein. It is pertinent to note that, this is for the first time, authors are reporting about the medicinal property of Macaflavanone E, Vibsanol B. As these three phytochemicals, namely, Belachinal, Macaflavanone E & Vibsanol B, have passed the ADMET test and 'Lipinski's Rule of 5s', they may be utilized in controlling disease caused via SARS-CoV2, in near future, after further *in vitro* and *in vivo* investigations.

## Acknowledgements

Authors would like to thank Mr. Jan Benzenberg, Incident Manager, Carrier Radio Access Networks (Germany), for providing the computational facility to carry out a molecular docking studies.

## Disclosure statement

The authors of this manuscript declare no conflict of interest.

## ORCID

Manoj Kumar Gupta  <http://orcid.org/0000-0003-1558-9471>  
Ramakrishna Vadde  <http://orcid.org/0000-0002-5223-7208>

## References

- Abraham, M. J., Murtola, T., Schulz, R., Páll, S., Smith, J. C., Hess, B., & Lindahl, E. (2015). GROMACS: High performance molecular simulations through multi-level parallelism from laptops to supercomputers. *SoftwareX*, 1-2, 19–25. doi:10.1016/j.softx.2015.06.001
- Altschul, S. F., Gish, W., Miller, W., Myers, E. W., & Lipman, D. J. (1990). Basic local alignment search tool. *Journal of Molecular Biology*, 215(3), 403–410. doi:10.1016/S0022-2836(05)80360-2
- Ashour, H. M., Elkhatib, W. F., Rahman, M. M., & Elshabrawy, H. A. (2020). Insights into the recent 2019 novel coronavirus (SARS-CoV-2) in light of past human coronavirus outbreaks. *Pathogens*, 9(3), 186. doi:10.3390/pathogens9030186
- Berger, O., Edholm, O., & Jähnig, F. (1997). Molecular dynamics simulations of a fluid bilayer of dipalmitoylphosphatidylcholine at full hydration, constant pressure, and constant temperature. *Biophysical Journal*, 72(5), 2002–2013. doi:10.1016/S0006-3495(97)78845-3
- Bertrand Teponno, R., Kusari, S., & Spitteller, M. (2016). Recent advances in research on lignans and neolignans. *Natural Product Reports*, 33(9), 1044–1092. doi:10.1039/C6NP00021E
- Binkowski, T. A., Naghibzadeh, S., & Liang, J. (2003). CASTp: Computed atlas of surface topography of proteins. *Nucleic Acids Research*, 31(13), 3352–3355. doi:10.1093/nar/gkg512
- Biovia, D. S. (2017). *Discovery studio visualizer*. San Diego, CA, USA.
- Curtis, K. M., Yount, B., & Baric, R. S. (2002). Heterologous gene expression from transmissible gastroenteritis virus replicon particles. *Journal of Virology*, 76(3), 1422–1434. doi:10.1128/JVI.76.3.1422-1434.2002
- Dhanda, S. K., Singla, D., Mondal, A. K., & Raghava, G. P. (2013). DrugMint: A webserver for predicting and designing of drug-like molecules. *Biology Direct*, 8(1), 28. doi:10.1186/1745-6150-8-28
- Donde, R., Gupta, M. K., Gouda, G., Kumar, J., Vadde, R., Sahoo, K. K., Dash, S. K., & Behera, L. (2019). Computational characterization of structural and functional roles of DREB1A, DREB1B and DREB1C in enhancing cold tolerance in rice plant. *Amino Acids*, 51(5), 839–853. doi:10.1007/s00726-019-02727-0
- Fischer, F., Stegen, C. F., Masters, P. S., & Samsonoff, W. A. (1998). Analysis of constructed E gene mutants of mouse hepatitis virus confirms a pivotal role for E protein in coronavirus assembly. *Journal of Virology*, 72(10), 7885–7894. doi:10.1128/JVI.72.10.7885-7894.1998
- Gouda, G., Gupta, M. K., Donde, R., Kumar, J., Vadde, R., Mohapatra, T., & Behera, L. (2020). Computational approach towards understanding structural and functional role of cytokinin oxidase/dehydrogenase 2 (CKX2) in enhancing grain yield in rice plant. *Journal of Biomolecular Structure and Dynamics*, 38(4), 1158–1110. doi:10.1080/07391102.2019.1597771
- Gupta, M. K., Donde, R., Gouda, G., Vadde, R., & Behera, L. (2019). De novo assembly and characterization of transcriptome towards understanding molecular mechanism associated with MYMIV-resistance in Vigna mungo - A computational study. *BioRxiv*, 844639. doi:10.1101/844639
- Gupta, M. K., & Vadde, R. (2019a). In silico identification of natural product inhibitors for  $\gamma$ -secretase activating protein, a therapeutic target for Alzheimer's disease. *Journal of Cellular Biochemistry*, 120(6), 10323–10336. doi:10.1002/jcb.28316
- Gupta, M. K., & Vadde, R. (2020a). Insights into the structure-function relationship of both wild and mutant Zinc transporter ZnT8 in human: A computational structural biology approach. *Journal of Biomolecular Structure & Dynamics*, 38(1), 137–151. doi:10.1080/07391102.2019.1567391
- Gupta, M. K., & Vadde, R. (2020b). A computational structural biology study to understand the impact of mutation on structure-function relationship of inward-rectifier potassium ion channel Kir6.2 in human. *Journal of Biomolecular Structure and Dynamics*. doi:10.1080/07391102.2020.1733666
- Gupta, M. K., Vadde, R., Donde, R., Gouda, G., Kumar, J., Nayak, S., Jena, M., & Behera, L. (2018). Insights into the structure-function relationship of brown plant hopper resistance protein, Bph14 of rice plant: A computational structural biology approach. *Journal of Biomolecular Structure and Dynamics*, 37(7), 1649–1617. doi:10.1080/07391102.2018.1462737
- Gupta, M. K., Vadde, R., Gouda, G., Donde, R., Kumar, J., & Behera, L. (2019). Computational approach to understand molecular mechanism involved in BPH resistance in Bt- rice plant. *Journal of Molecular Graphics and Modelling*, 88, 209–220. doi:10.1016/j.jmkgm.2019.01.018
- Gupta, M. K., Vadde, R., & Sarojamma, V. (2020). Curcumin - A novel therapeutic agent in the prevention of colorectal cancer. *Current Drug Metabolism*, 20(12), 977–987. doi:10.2174/1389200220666191007153238
- Ramphul, K., & Mejias, S. G. (2020). Coronavirus disease: A review of a new threat to public health. *Cureus*, 12(3), e7276. doi:10.7759/cureus.7276
- Krijnse-Locker, J., Ericsson, M., Rottier, P. J., & Griffiths, G. (1994). Characterization of the budding compartment of mouse hepatitis virus: Evidence that transport from the RER to the Golgi complex requires only one vesicular transport step. *The Journal of Cell Biology*, 124(1), 55–70. doi:10.1083/jcb.124.1.55
- Li, G., Fan, Y., Lai, Y., Han, T., Li, Z., Zhou, P., Pan, P., Wang, W., Hu, D., Liu, X., Zhang, Q., & Wu, J. (2020). Coronavirus infections and immune responses. *Journal of Medical Virology*, 92(4), 424–432. doi:10.1002/jmv.25685
- Lin, Y.-C., Wang, C.-C., Chen, I.-S., Jheng, J.-L., Li, J.-H., & Tung, C.-W. (2013). TIPdb: A database of anticancer, antiplatelet, and antituberculosis phytochemicals from indigenous plants in Taiwan. *The Scientific World Journal*, 2013, 1–4. doi:10.1155/2013/736386

- Mehrnejad, F., & Chaparzadeh, N. (2008). Structural and dynamical studies of humanin in water and TFE/water mixture: A molecular dynamics simulation. *Journal of Biomolecular Structure and Dynamics*, 26(2), 255–262. doi:10.1080/07391102.2008.10507241
- Morris, G. M., Huey, R., Lindstrom, W., Sanner, M. F., Belew, R. K., Goodsell, D. S., & Olson, A. J. (2009). AutoDock4 and AutoDockTools4: Automated docking with selective receptor flexibility. *Journal of Computational Chemistry*, 30(16), 2785–2791. doi:10.1002/jcc.21256
- Nieto-Torres, J. L., DeDiego, M. L., Verdiá-Báguena, C., Jimenez-Guardeño, J. M., Regla-Nava, J. A., Fernandez-Delgado, R., Castaño-Rodríguez, C., Alcaraz, A., Torres, J., Aguilera, V. M., & Enjuanes, L. (2014). Severe acute respiratory syndrome coronavirus envelope protein ion channel activity promotes virus fitness and pathogenesis. *PLoS Pathogens*, 10(5), e1004077. doi:10.1371/journal.ppat.1004077
- Perlman, S., & Netland, J. (2009). Coronaviruses post-SARS: Update on replication and pathogenesis. *Nature Reviews Microbiology*, 7(6), 439–450. doi:10.1038/nrmicro2147
- Pervushin, K., Tan, E., Parthasarathy, K., Lin, X., Jiang, F. L., Yu, D., Vararattanavech, A., Soong, T. W., Liu, D. X., & Torres, J. (2009). Structure and Inhibition of the SARS coronavirus envelope protein ion channel. *PLoS Pathogens*, 5(7), e1000511. doi:10.1371/journal.ppat.1000511
- Rani, Y. G., & Lakshmi, B. S. (2019). Structural insight into the antagonistic action of diarylheptanoid on human estrogen receptor alpha. *Journal of Biomolecular Structure and Dynamics*, 37(5), 1189–1203. doi:10.1080/07391102.2018.1453378
- Regla-Nava, J. A., Nieto-Torres, J. L., Jimenez-Guardeño, J. M., Fernandez-Delgado, R., Fett, C., Castaño-Rodríguez, C., Perlman, S., Enjuanes, L., & DeDiego, M. L. (2015). Severe acute respiratory syndrome coronaviruses with mutations in the E protein are attenuated and promising vaccine candidates. *Journal of Virology*, 89(7), 3870–3887. doi:10.1128/JVI.03566-14
- Rota, P. A., Oberste, M. S., Monroe, S. S., Nix, W. A., Campagnoli, R., Icenogle, J. P., Peñaranda, S., Bankamp, B., Maher, K., Chen, M.-H., Tong, S., Tamin, A., Lowe, L., Frace, M., DeRisi, J. L., Chen, Q., Wang, D., Erdman, D. D., Peret, T. C. T., ... Bellini, W. J. (2003). Characterization of a novel coronavirus associated with severe acute respiratory syndrome. *Science*, 300(5624), 1394–1399. doi:10.1126/science.1085952
- Schoeman, D., & Fielding, B. C. (2019). Coronavirus envelope protein: Current knowledge. *Virology Journal*, 16(1), 69. doi:10.1186/s12985-019-1182-0
- Schüttelkopf, A. W., & van Aalten, D. M. F. (2004). PRODRG: A tool for high-throughput crystallography of protein–ligand complexes. *Acta Crystallographica Section D Biological Crystallography*, 60(8), 1355–1363. doi:10.1107/S0907444904011679
- Shang, W., Yang, Y., Rao, Y., & Rao, X. (2020). The outbreak of SARS-CoV-2 pneumonia calls for viral vaccines. *NPJ Vaccines*, 5(1), 1–3. doi:10.1038/s41541-020-0170-0
- Tandon, G., Jaiswal, S., Iqbal, M. A., Kumar, S., Kaur, S., Rai, A., & Kumar, D. (2015). Evidence of salicylic acid pathway with EDS1 and PAD4 proteins by molecular dynamics simulation for grape improvement. *Journal of Biomolecular Structure and Dynamics*, 33(10), 2180–2191. doi:10.1080/07391102.2014.996187
- Tooze, J., & Tooze, S. A. (1985). Infection of AtT20 murine pituitary tumour cells by mouse hepatitis virus strain A59: Virus budding is restricted to the Golgi region. *European Journal of Cell Biology*, 37, 203–212.
- Torres, J., Maheswari, U., Parthasarathy, K., Ng, L., Liu, D. X., & Gong, X. (2007). Conductance and amantadine binding of a pore formed by a lysine-flanked transmembrane domain of SARS coronavirus envelope protein. *Protein Science*, 16(9), 2065–2071. doi:10.1110/ps.062730007
- Venkatagopalan, P., Daskalova, S. M., Lopez, L. A., Dolezal, K. A., & Hogue, B. G. (2015). Coronavirus envelope (E) protein remains at the site of assembly. *Virology*, 478, 75–85. doi:10.1016/j.virol.2015.02.005
- Verdiá-Báguena, C., Nieto-Torres, J. L., Alcaraz, A., Dediego, M. L., Enjuanes, L., & Aguilera, V. M. (2013). Analysis of SARS-CoV E protein ion channel activity by tuning the protein and lipid charge. *Biochimica Et Biophysica Acta (Bba) - Biomembranes*, 1828(9), 2026–2031. doi:10.1016/j.bbame.2013.05.008
- Verdiá-Báguena, C., Nieto-Torres, J. L., Alcaraz, A., DeDiego, M. L., Torres, J., Aguilera, V. M., & Enjuanes, L. (2012). Coronavirus E protein forms ion channels with functionally and structurally-involved membrane lipids. *Virology*, 432(2), 485–494. doi:10.1016/j.virol.2012.07.005
- Westerbeck, J. W., & Machamer, C. E. (2019). The infectious bronchitis coronavirus envelope protein alters Golgi pH to protect the spike protein and promote the release of infectious virus. *Journal of Virology*, 93(11), e00015-19. doi:10.1128/JVI.00015-19
- Wilson, L., McKinlay, C., Gage, P., & Ewart, G. (2004). SARS coronavirus E protein forms cation-selective ion channels. *Virology*, 330(1), 322–331. doi:10.1016/j.virol.2004.09.033
- Wolf, M. G., Hoefling, M., Aponte-Santamaría, C., Grubmüller, H., & Groenhof, G. (2010). g\_membed: Efficient insertion of a membrane protein into an equilibrated lipid bilayer with minimal perturbation. *Journal of Computational Chemistry*, 31(11), 2169–2174. doi:10.1002/jcc.21507